Mar Geophys Res (2011) 32:313–329
DOI 10.1007/s11001-010-9103-z

ORIGINAL RESEARCH PAPER

The 1888 shoreline landslide and tsunami in Trondheimsfjorden, central Norway

J.-S. L'Heureux · S. Glimsdal · O. Longva · L. Hansen · C. B. Harbitz

Received: 30 March 2010 / Accepted: 12 October 2010 / Published online: 23 October 2010

Abstract The 1888 landslide and tsunami along the shore of the bay of Trondheim, central Norway, killed one person and caused major damage to port facilities. Recent bathymetric surveys, high-resolution seismic profiles and CPTU piezocone tests provide detail information about the morphology of the seafloor and landslide mechanisms, which can be used in tsunami simulations. Based on our integrated data set we suggest the 1888 sequence of events started with an initial underwater landslide near-shore, by detachment along a weak clayey sediment layer. Geomorphology indicates the landslide transformed rapidly into a debris flow, which subsequently triggered slope failures on the flanks of a deep underwater channel. One of the slope failures is associated with the triggering of the 1888 tsunami wave, with documented run-up heights of several meters. The interpreted sequence of events is supported by eyewitness testimony and further validated by slope stability analysis, slide dynamics modelling and 2D tsunami simulations.

Keywords Shoreline · Fjord · Submarine landslide · Slope stability · Mobility · Tsunami

J.-S. L'Heureux (✉) · O. Longva · L. Hansen
Geological Survey of Norway, Trondheim, Norway
e-mail: jean.lheureux@ngu.no

S. Glimsdal · C. B. Harbitz
Norwegian Geotechnical Institute, Oslo, Norway

J.-S. L'Heureux · S. Glimsdal · O. Longva · L. Hansen · C. B. Harbitz
International Centre for Geohazards, Oslo, Norway

Introduction

Submarine landslides are widely recognized as a potential hazard to offshore development and coastal infrastructures (e.g. Locat and Lee 2002), as well as a source for destructive tsunamis (e.g. Tappin 2009). Large landslides on the continental margin have proven devastating to coastal communities (e.g. 1929 Grand Banks landslide and tsunami; Piper and Asku 1987). However, coastal and near-shore landslides often represent a greater hazard to communities, because of their proximity to the shoreline.

The bay of Trondheim, central Norway, is well suited for the study of near-shore mass wasting processes and their consequences (Fig. 1). Here, landslides have occurred repeatedly during the last century causing damages to port facilities as well as loss of life (Bjerrum 1971; Emdal et al. 1996; L'Heureux et al. 2007). The most devastating submarine landslide in this fjord deltaic setting occurred April 23rd, 1888, and was accompanied by a 5–7 m high tsunami wave (Bjerrum 1971). The characteristics of the 1888 event in Trondheim is similar to other historical submarine landslide events, which showed a sequence of offshore initiation, retrogression close to, or across, the shoreline, and generation of tsunami waves [e.g. 1975 Kitimat event in British Columbia (Prior et al. 1982) and the 1979 Nice catastrophe in France (Dan et al. 2007)]. For many of these events it has been difficult to pinpoint the causes for slope failures and the generation of tsunami waves. As the population continues to migrate toward the coastlines and the impacts of these hazards are expected to grow, there is a need for a better understanding of these types of coastal hazards.

In the present paper, the 1888 event in Trondheim is studied to show one example of the complexity of mass-wasting processes in near-shore and coastal environments.

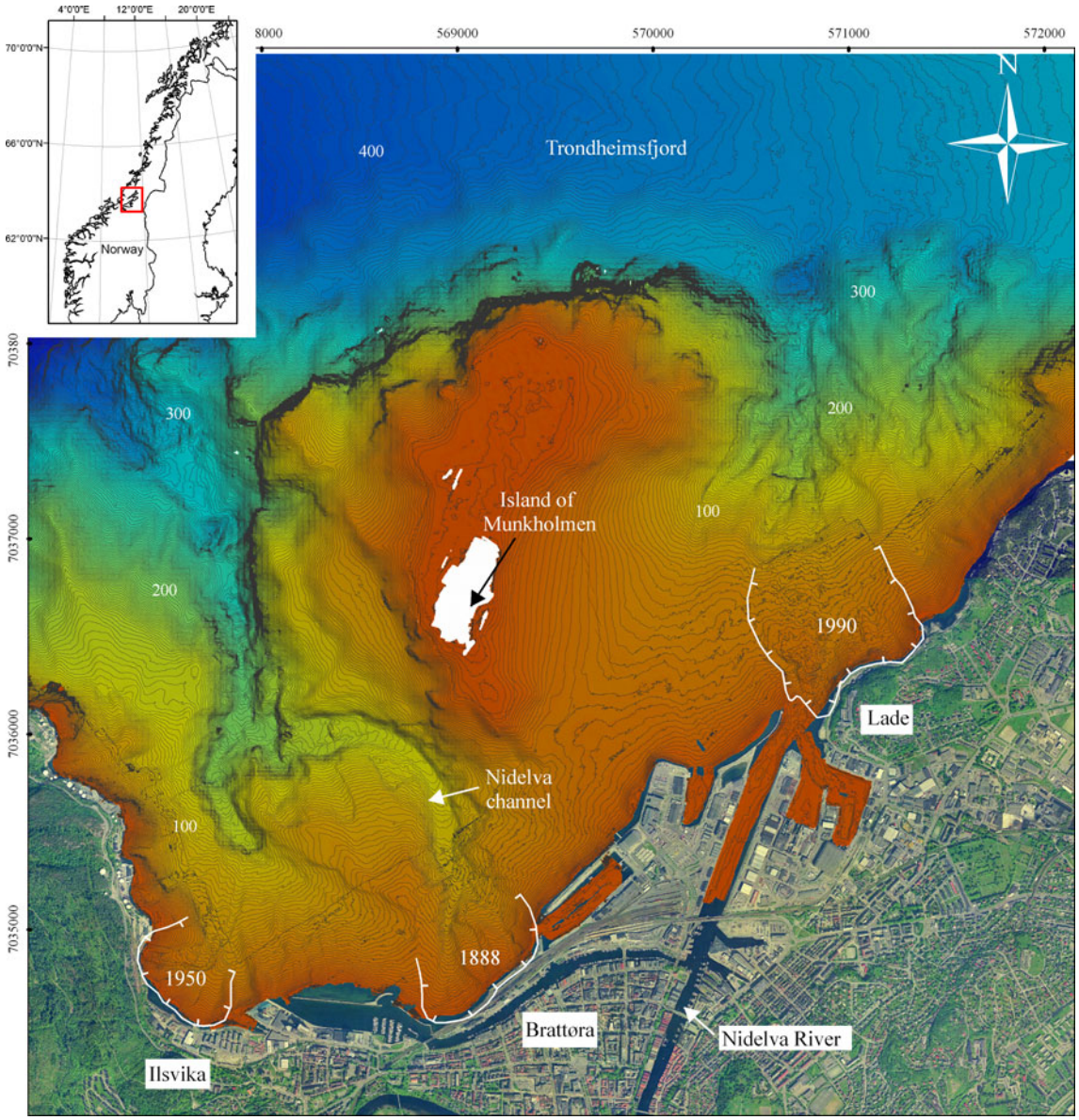

Fig. 1 Location of the study area with bathymetric data from the embayment of Trondheim, central Norway (UTM zone 32N)

The study is based on a set of multibeam bathymetric data, high-resolution seismic data, cores and in situ piezocone tests. The aim of this study is to reconstruct and discuss the sequence of events which led to the 1888 landslide and tsunami in Trondheim. The evaluation includes a review of data, analysis of the seafloor morphology, slope stability analyses and tsunami modelling.

Setting

Bedrock around Trondheim is dominated by Precambrian-Silurian westward dipping low-grade metamorphic, volcanic rocks, especially green schist and tuff (Wolff 1976). During repeated glaciations, bedrock was eroded along weakness zones and shaped the present landscape of valleys and fjords, including the present valley at Trondheim. Bedrock is exposed locally on land and at sea bed in the study area (L'Heureux et al. 2009a). Along the shoreline of Trondheim, bedrock is covered by a 125-m thick succession consisting of glacio-marine deposits, prodelta sediments, steeply dipping delta foresets, and gravel beach (L'Heureux et al. 2010; Fig. 2). The glacio-marine and marine sediments were deposited during the end of the last glacial period prior to ~10,000 ^{14}C BP and the early Holocene period, respectively (Reite 1995; Lyså et al. 2007). The area was thereafter subjected to glacio-isostatic rebound, which caused rapid fall of relative sea-level and a

continuous, northwards progradation of the river mouth delta during the Holocene (Reite et al. 1999). Delta-derived and failure-generated sediment gravity flows were especially active outside the river mouth during the Mid- to Late-Holocene, and this promoted the incision of the Nidelva channel as shown in Fig. 1 (L'Heureux et al. 2009a). Since 3,000–2,000 cal. years. BP, the submarine channel has not been linked to any major fluvial source (L'Heureux et al. 2009a).

Harbour development and land reclamation along the Nidelva river delta started in 1875 through filling of large near-shore areas. Since then at least three major landslide events have taken place along the shoreline of Trondheim bay (Skaven-Haug 1955; Emdal et al. 1996; L'Heureux et al. 2007). The 1888 landslide occurred in the central part of the bay at Brattøra, whereas the landslides in 1950 and 1990 occurred in the west at Ilsvika and in the east of the bay at Lade, respectively (Fig. 1). Earlier work by Bjerrum (1971) and Emdal et al. (1996) suggested that landslides along the shoreline of the bay were the result of a collapse and liquefaction of loose sandy material. A recent study by L'Heureux et al. (2010) showed, however, that landslides in the bay tend to occur along distinct planes associated with weak, laminated, clay-rich beds in the delta front and prodelta sequences.

Even though it has been difficult to pinpoint the causes for landslide in the near-shore area of Trondheim, it is generally agreed that these result from a combination of human activities (e.g. placement of fill along the shore and blasting) and natural factors (e.g. erosion, high sedimentation rates and unfavourable groundwater conditions) (Bjerrum 1971; Emdal et al. 1996; L'Heureux et al. 2007, 2010). In the present study area, no historical earthquakes have been registered and the area is regarded as having one of Scandinavia's lowest seismicity (Dehls et al. 2000). The seismicity of Norway is low to intermediate in intensity and is related to both tectonics and post-glacial rebound (Gölke et al. 1996; Pascal and Gabrielsen 2001).

The 1888 catastrophe in the bay of Trondheim

From the testimony of 20 eye witnesses, Skaven-Haug (1955) concluded the 1888 event started with the appearance of a flood wave in the fjord approximately halfway between the island of Munkholmen and Ilsvika (Fig. 1). Records indicate that the wave propagated towards the shoreline and first struck land at Ilsvika. Some minutes later another wave climbed over a 5–7 m high embankment fill at Brattøra and, just as it receded, a 170 m long portion of the railway station slumped into the fjord (Fig. 3). Three railway tracks were washed away and one man perished in the event. In the following hours minor slope failures took place east of the main scar. The incident occurred during a spring low tide and no construction activity had taken place at Brattøra since 1880 (Skaven-Haug 1955; Bjerrum 1971). Initial work by Skaven-Haug (1955) and Bjerrum (1971) suggested that the 1888 landslide at Brattøra was initiated by a landslide at a great depth in the fjord. However, no thorough explanation could be given for the occurrence of such a landslide. During the winter of 1888 snow accumulation twice above the normal values were recorded in Trondheim (data from the Norwegian Meteorological Institute 2009). These data have previously not been considered during evaluation of the 1888 event.

Data

Bathymetric and geophysical investigations

A set of bathymetric data from the bay of Trondheim was acquired in 2009 by means of 250 kHz interferometric sonar system (GeoAcoustics) mounted onboard of the R/V Seisma. A stabilizer system (TSS DM) was used to compensate and adjust for the pitch and roll of the vessel. This also allowed heel and trim adjustment of the ship in real-time. Sound velocity in the water adjacent to the

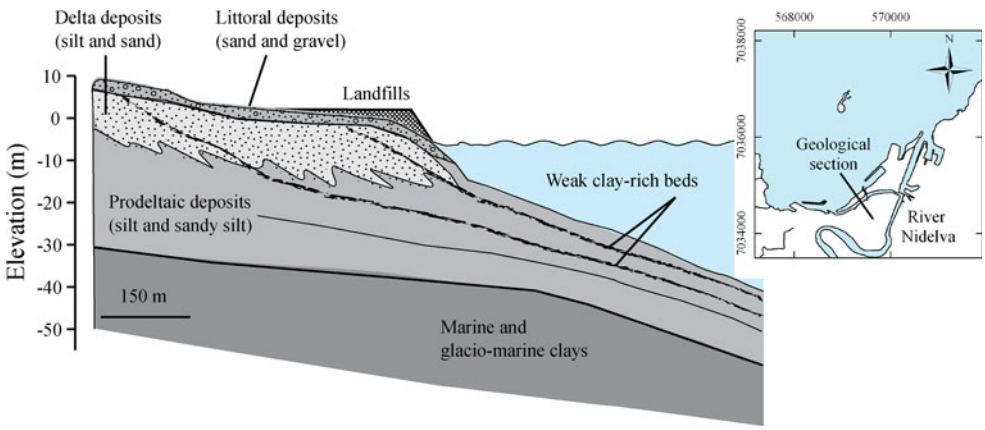

Fig. 2 Schematic geological cross-section of the Nidelva delta, from L'Heureux et al. (2010)

Fig. 3 Scene at Brattøra, Trondheim, following the 1888 landslide and tsunami. (Photo: Courtesy of Hifling Rasmussen)

transmitters/receivers was measured with help of a Valport 650 Sound Velocity Profiler (SVP). These measurements were performed systematically to obtain optimal velocity profiles for calculation of water depths. During the cruise, positioning was performed by means of differential GPS positioning system with an accuracy of ± 1 meter. Tidal variations were measured during surveying and the tidal correction was merged into the survey file during processing. In this study the bathymetric data are presented at a grid spacing of 1 m.

In the period 2003–2009, a dense network of high-frequency (3.5 kHz) seismic data was acquired using a parametric sub-bottom profiler (TOPAS system). Processing of the data included the application of a band-pass filter and corrections for sea-level variations. The range of resolution for the parametric sub-bottom profiler is typically of 10 cm or better (Kongsberg Defense and Aerospace 2004). Two-way travel time was converted to water depth and sediment thickness using a constant velocity of 1,450 ms^{-1}.

Core data and insitu geotechnical testing

Thirty gravity cores, 47 niemestoe cores and one Calypso core (14.5 m) have been collected from the seafloor of the embayment since 2003. The location of the cores used in this study is shown in Fig. 4. In the laboratory the cores were X-rayed and split to describe lithology and sedimentary structures. A wide range of geotechnical tests were performed, including: grain size analysis, water content, liquid and plastic limits, undrained shear strength (s_u) using the Swedish Fall cone, and three undrained triaxial tests (CIU tests). Other results from these cores are presented in L'Heureux et al. (2009a, 2010) and Hansen et al. (2010). A Remotely Operated Vehicle (ROV) was also used in 2008 for precise sampling and observation of the seafloor at a few places in the study area.

Data in this study is complemented by in situ piezocone tests (CPTU) carried out by consulting geo-technicians between 2003 and 2008, in relation with construction works along the shore of Trondheim. The CPTU tests allow for continuous measurement of tip resistance (q_c), sleeve friction (f_s) and pore pressure behind the cone (u_2) during penetration. This information can be used for lithological description and for determination of shear strength and soil stiffness (Lunne et al. 1997). Moreover, as the pore-water pressure around a penetrating cone influences the measured tip resistance and the sleeve friction, it is generally recommended for q_c values to be reported as total resistance q_t whenever possible (Campanella et al. 1983). This correction, as shown in Eq. 1, is especially important in soft clays and silts where q_c is generally low and the excess pore pressure is high:

$$q_t = q_c + u_2(1 - a) \tag{1}$$

where a is the cone area ratio (Robertson 1990). In this study we make use of CPTU data to estimate the undrained shear strength of soft and normally consolidated sediments. Reliable shear strength parameters can be derived from the in situ CPTU tests using an empirical relationship of the form:

$$s_u = \frac{(q_c - \sigma_{v0})}{N_k} \tag{2}$$

where N_k is an empirical cone factor (assumed to be equal to 15 for normally consolidated clay) and σ_{v0} is the total in situ vertical stress (Lunne et al. 1997). In the case where coarser sediments are present (e.g. silt, sand and gravel) CPTU data can also be used to derive effective strength parameters, such as the angle of friction (φ') and the cohesion intercept (c'), by using charts proposed by Senneset et al. (1988).

Morphology

Water depth in the central part of the bay of Trondheim is 40–50 m and acts as a saddle, dividing the bay into an eastern and western part (Fig. 1). The present-day mouth of the Nidelva River is located in the eastern part of the embayment. To the west, the Nidelva submarine channel can be followed from near the shoreline north of Brattøra and down to a depth of 450 m in the central part of the fjord basin (Fig. 1). The width of the channel varies from 100 to 200 m and the slope of the channel floor is between 4 and 6°. The shallowest reach of the channel is characterized by a 500-m long linear segment followed by an abrupt change in direction (~90° bend) towards the west. The outer bend is bordered by a bedrock high at the Munkholmen Island. Bedrock outcrops are also observed in

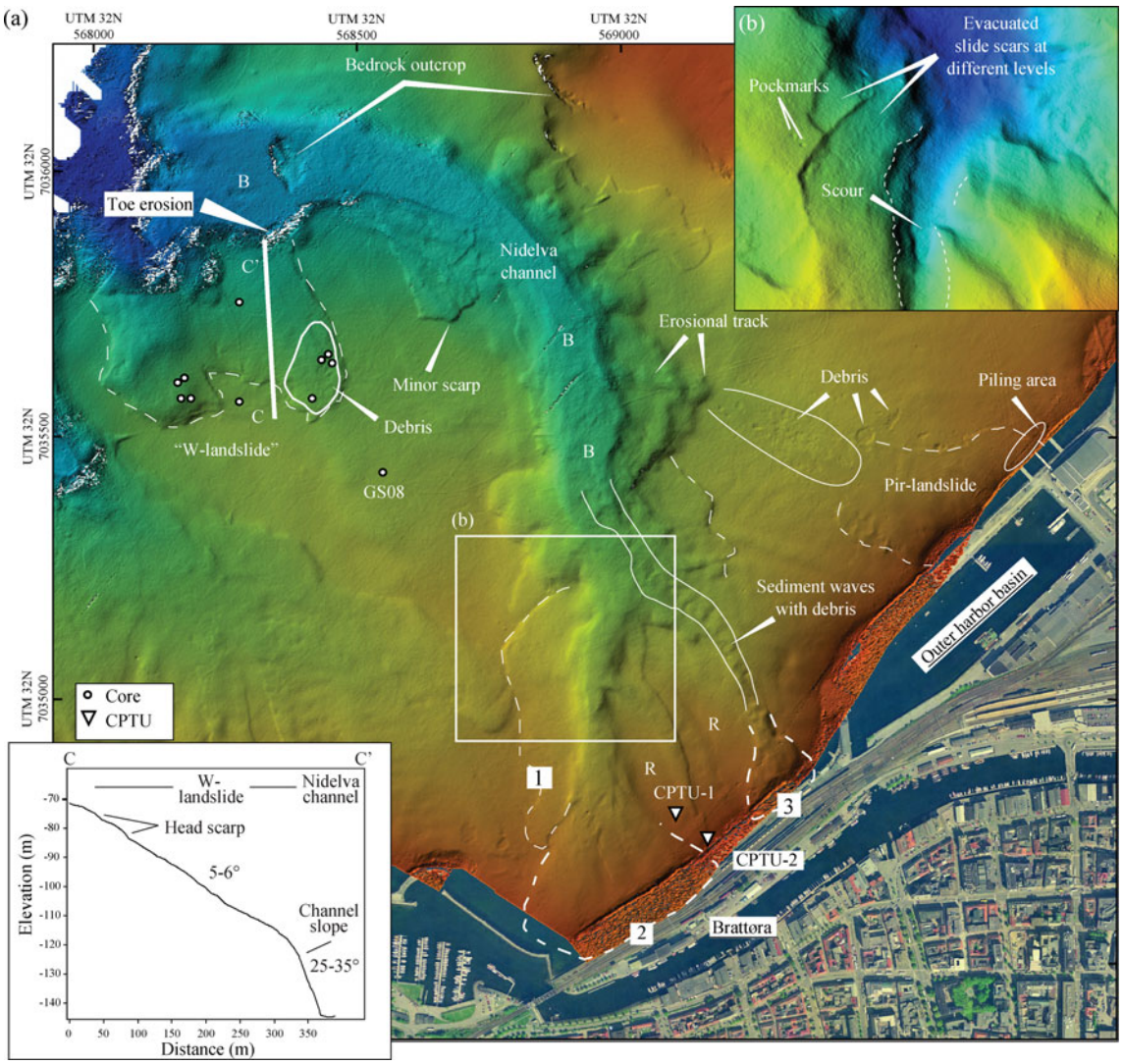

Fig. 4 **a** Identification of the main morphological signatures from the seafloor outside Brattøra and along the Nidelva channel. The position of cores and CPTU tests used in this study are shown. **b** Close up view of the seafloor morphology showing evacuated slide scars at different stratigraphic levels, pockmarks upslope of the escarpments and a deep scour feature. **c** Topographic profile across the W-landslide showing the 8-m high head scarp and the steep slope section (erosion) at the channel flank. (R: ridge of un-failed slope)

the submarine channel (Fig. 4). Observation by means of an ROV showed rectangular shaped, rock blocks (>1 m in diameter) at different emplacement in the submarine channel (see "B", Fig. 4).

Detailed swath bathymetry imaging shows numerous slide scars in the western part of the bay (Fig. 4). Some of the observed scars are distinct whereas others are more vague and draped by sediments. The highest density of scars is observed on the steeper sides of the channel (i.e. northern/eastern flank), especially in the ~90° bend. Larger scars are also observed on the southern/western flank (e.g. W landslide, Fig. 4), at the head of the channel (i.e. Brattøra landslide) and along the shore outside the channel (e.g. Pir-landslide).

Brattøra landslide

The seafloor at the head of the Nidelva channel, north of Brattøra, exhibits complex morphology with several scars with back walls ranging from 3 to 10 m in height (see 1, 2 and 3, Fig. 4). Two distinct seafloor morphologies, one smooth and one rough, are seen within the various scars. The smooth seafloor corresponds to evacuated landslide scar devoid of debris (e.g. scar 1, Fig. 4). In contrast, the rougher seafloor represents a cover of landslide debris up to a few meters thick (e.g. scars 2, 3, Fig. 4) and displays undulations interpreted as sediment waves with some debris (Fig. 4). Between the shore-parallel escarpments 2 and 3 at Brattøra, is an unfailed slope segment slightly

eroded at the surface and which dips at an angle of 5–6° (see "R" in Figs. 4 and 5a). A high resolution seismic profile through the un-failed ridge shows parallel-bedded reflections, one of which corresponds to the level of the evacuated slide scar 2 (Fig. 5b). Pockmarks are also present at some locations upslope of the scars whereas an erosive element, interpreted as a scour, is observed north of scar 2 (Fig. 4b).

The smooth planar surfaces inside the evacuated slide scars outside Brattøra, combined with the presence parallel-bedded sediments, suggests the influence of weaker beds on the mechanism of failure and on the location of sliding. Internal scars and evacuated surfaces at different levels indicate the presence of weak layers at different stratigraphic levels (Fig. 4b). The seafloor morphology is also indicative of retrogressive landslide behaviour since the sediments that originated upslope near the shoreline cover the base of the scars downslope. The sediment waves and scouring observed in front of the near-shore escarpments are indicative of high energy sediment flow funnelled into the Nidelva channel following failure.

Pir-landslide

Seaward of the pier at the outer harbor basin, bathymetric data displays a 1- to 3-m high landslide escarpment which gradually disappears in the steeper upslope section at the shoreline (Fig. 4). The seafloor slope angle near the shoreline reaches values of 25°, but rapidly decreases to about 7–10° at less than 75 m to the north. Blocks and slide debris occur in front and at the sides of the slide scar, with the largest block having a diameter of 35 m and a height of 1.5 m (Fig. 4). Some of the blocks originating upslope have travelled over the lowermost section of the scar downslope.

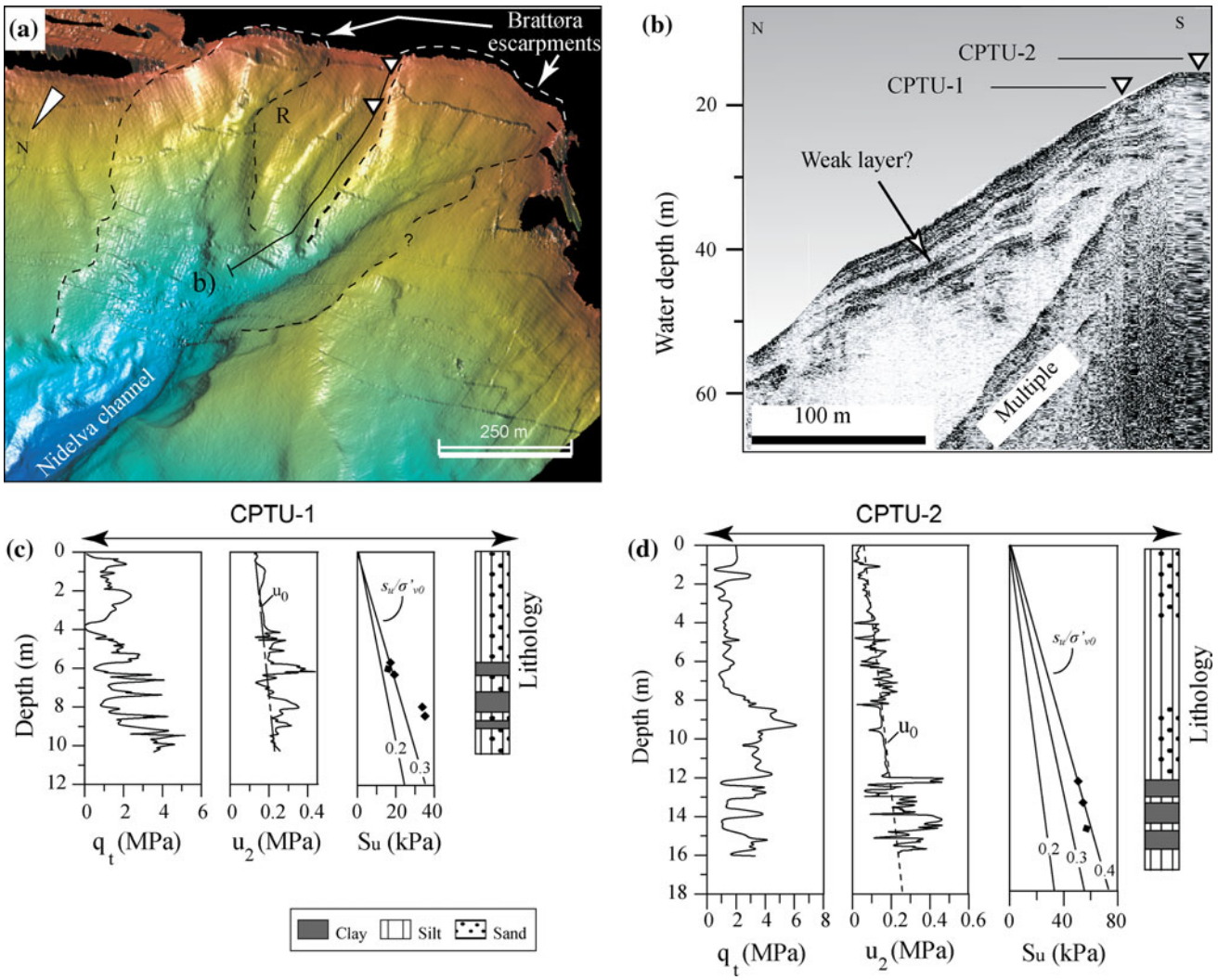

Fig. 5 **a** 3D shaded relief image of the Brattøra landslide with view angle towards the shoreline (south). **b** High resolution seismic profile through the intact sediment ridge (R) shown in (**a**). Results from CPTU-1 and CPTU-2 are shown in (**c**) and (**d**), respectively

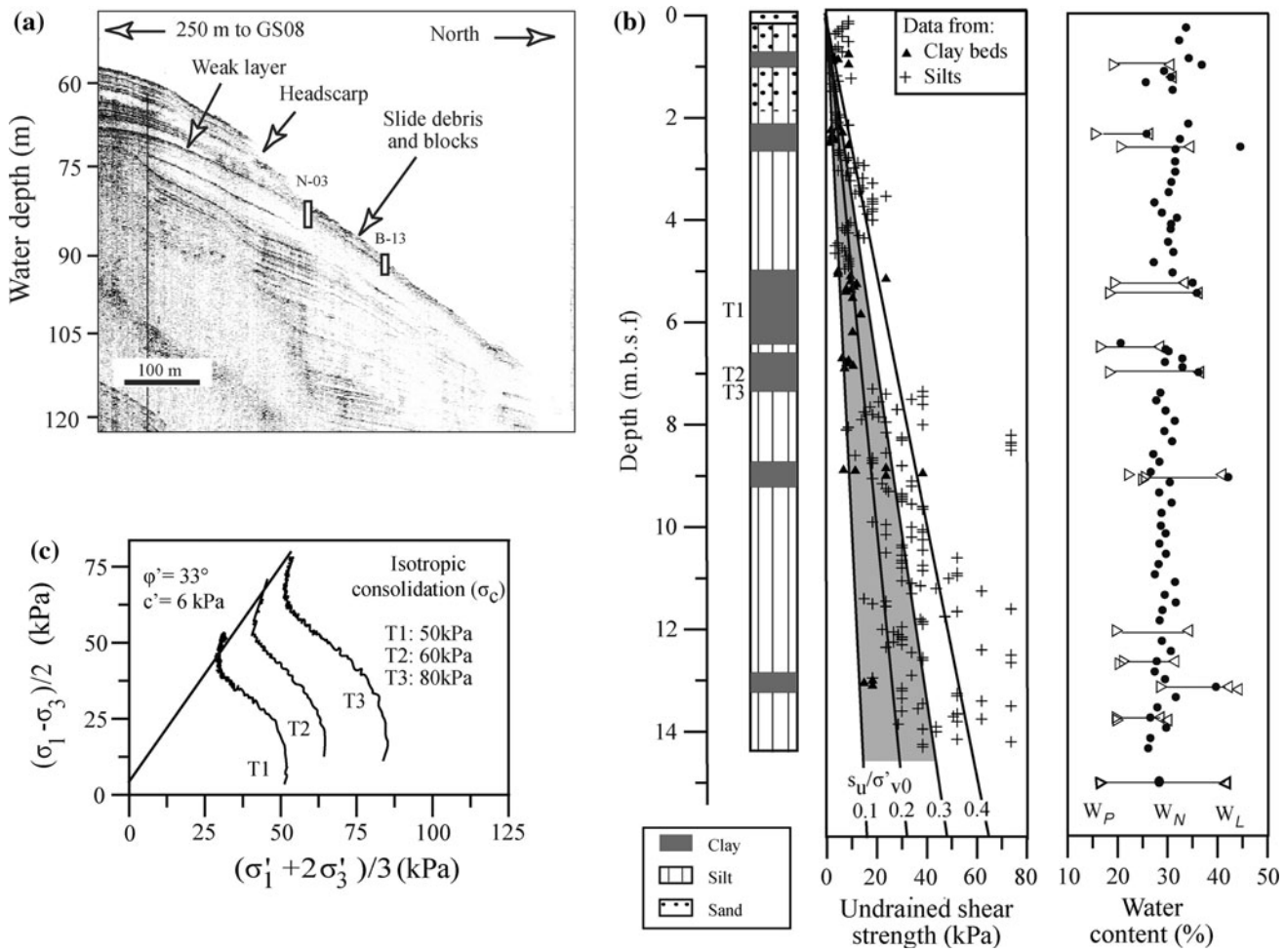

Fig. 6 **a** Part of a high-resolution seismic line through the W-landslide which shows a distinct high amplitude reflection (weak layer) correlating to the landslide failure surface. The location of the seismic line corresponds nearly to profile C–C' in Fig. 4. **b** Lithology, undrained shear strength and water content from piston core GS08 (see location in Fig. 4a). **c** Results from three triaxial tests on laminated clay-rich beds from core GS08

Most of the debris and blocks have however been transported into deeper water into the Nidelva channel where an erosional track is observed (Fig. 4). Such erosion by the sediment gravity flow following the Pir-landslide most likely affected the stability of slopes downstream.

The retrogressive process during the Pir-landslide gradually ceased as it reached coarser and stronger material close to the shoreline (c.f. landfills, coarse sand and gravels, Fig. 2). Because of this, and because it did not cause any damage to coastal infrastructure, the Pir-landslide never was noticed by the harbor authorities. It can be considered that this landslide is at least 8 years old since it is present on bathymetric data collected in 2001 (Bjerkli, personal communication). The triggering of this landslide could also be attributed to fillings and/or to the driving of piles during the construction of the pier outside the outer harbor basin in 1994. This is because the main slide scar passes through the piling area (Fig. 4).

W-landslide

The largest slide scar along the flanks of the Nidelva channel is situated 2 km off-shore at a water depth of 80–160 m and is named the W-landslide (Fig. 4). The head scarp varies between 5 and 10 m in height and border a smooth planar surface dipping at 5 and 6°. At one location, landslide debris that originated upslope in proximity of the head scarp drapes the sliding surface downslope, indicating retrogressive landslide mechanism (Fig. 4). At the base of the W-landslide, along the flank of the Nidelva channel, steep slope gradients are observed (25–35°) (Fig. 4). This indicates that toe erosion and undercutting of the slope may have been important for triggering the landslide. Data from high-resolution seismic profiles show several, parallel reflections, upslope of the W-landslide escarpment (Fig. 6a). Some of these marked reflections correlate well to the smooth and

planar slide surface and testify to weaker layers involved in the sliding process.

The total volume of the W-landslide can be estimated to $\sim 1.45 \times 10^6$ m^3 based on the surface affected by the landslide (18,125 m^2) and using an average height of removed material (8 m). The location of the W-landslide corresponds well with the location of the initial flood wave that was witnessed in the fjord in 1888 (Skaven-Haug 1955).

Geological and geotechnical properties

Brattøra site

Two in situ piezocone tests (CPTU-1 and CPTU-2) were performed on the seabed off Brattøra, on the delta foreslope, through the intact sediment ridge (Fig. 5). The results show loose to medium dense sand and silty sand layers interbedded with softer, clayey beds at a depth of 6–8 m in CPTU-1 and at a depth of 12–15 m in CPTU-2. The integration of high-resolution seismic data and CPTU data shows that the coarser deltaic sediments are thinning northwards towards the fjord (Fig. 5b). The depth of the softer clayey beds (c. 6 m) correlates to a specific seismic unit on the same figure. This zone corresponds to the level of the sliding plane of scar 2 at Brattøra and is interpreted as a weak layer (Fig. 5b). Shear strength parameters derived from the in situ CPTU tests, and using Eqs. 1 and 2, show that s_u is lowest in the clayey layer found at a depth of 6 m in CPTU-1 (Fig. 5c). The undrained shear strength ratio (s_u/σ'_{v0}) at this depth is close to 0.3 and is representative of soft normally consolidated material. Results from CPTU-2 show a higher s_u for a similar clayey layer, likely because of an increase in confining stresses (burial depth) (see CPTU-2, Fig. 5d). In general, the sensitivity of the thin clayey layers varies from 5 to 7 onshore at Brattøra (Statens Vegvesen 2004a, b).

Four wells were drilled onshore at Brattøra (4–5 m.a.s.l.) in 2008 for monitoring the groundwater levels prior to road construction (Statens Vegvesen 2008). These levels were recorded for a period of two months between the end of February 2008 and the end of April 2008. Readings were taken two times a day in the deltaic sand deposits immediately below and above a 4 meter-thick soft clayey bed. The groundwater level measured above the clayey layer was hydrostatic and varied from 1.10 to 1.80 m.a.s.l. Records below the clayey layer at a depth of 10 m indicated a higher groundwater level, varying between 2.30 and 2.54 m.a.s.l. This corresponds to an excess pore-pressure ratio (r_u) varying from 0.35 to 0.40 below the clayey layer. Such high excess pore-pressures indicate that the groundwater conditions and seepage from land to fjord may affect the stability of near-shore slopes at Brattøra.

W-landslide site

Core GS08, collected upslope of the W-landslide, displays 2 m of silty sand covering brownish silts and laminated, light-grey, clay-rich beds (Fig. 6b). Similar clay-rich beds were collected from cores N-03 and B-13, inside the W-landslide scar (Fig. 6a). The centimetre to meter thick clayey beds are clearly marked by an increase in water content (equivalent to or higher than the liquid limit) and a lowering in undrained shear strength (s_u). For these beds, s_u/σ'_{v0} varies between 0.1 and 0.3 with an average of 0.2, being representative for soft normally consolidated material. L'Heureux et al. (2010) showed that the sensitivity of these soft, clayey beds varies between 3 and 17 in the fjord.

Three triaxial tests (i.e. T1, T2 and T3) were performed on clay-rich samples from GS08 and the results are presented in Fig. 6c. The samples were consolidated close to their assumed in situ effective stresses (T1 = 50 kPa, T2 = 60 kPa and T3 = 80 kPa). The tests provide a failure envelope indicating an effective friction angle (φ') of 33° and a cohesion intercept (c′) around 6 kPa.

Several cores have been collected from the W-landslide area (Fig. 4a). These cores have previously been used to show that the failure plane of the W-landslide corresponds to a clay-rich bed similar to that collected in core GS08 at a depth interval of 5.0–7.3 m (L'Heureux et al. 2009a, 2010). The cores show 3–13 cm of bioturbated sediments on top of the slide plane and/or other sediments interpreted as debris. Bioturbated sediments in cores nearby show an accumulation rate of 1.7–2.0 mm/year (L'Heureux et al. 2009a; Hansen et al. 2010). Applying this accumulation rate for the top sediments inside the slide scar does not give an accurate age estimate but confirms that the W-landslide is relatively recent and could fit well with the 1888 landslide and tsunami event.

Stability analysis

Inputs and considerations

Slope stability analyses of the Brattøra and W- landslides are presented in this section in order to discuss the potential failure scenarios and to constrain the sequence of events which led to the 1888 catastrophe in the bay of Trondheim. The commercially available slope stability package Slope/W was used to perform the 2D limit equilibrium back-analyses (GEO-SLOPE 2008). Since no earthquake or vibrations were recorded prior to the 1888 event, the slopes are modelled under the effect of gravitational stresses only (i.e. static forces). The output factor of safety (FoS; i.e. the ratio between the average resisting shear strength of the soil and the average shear stress mobilized along a

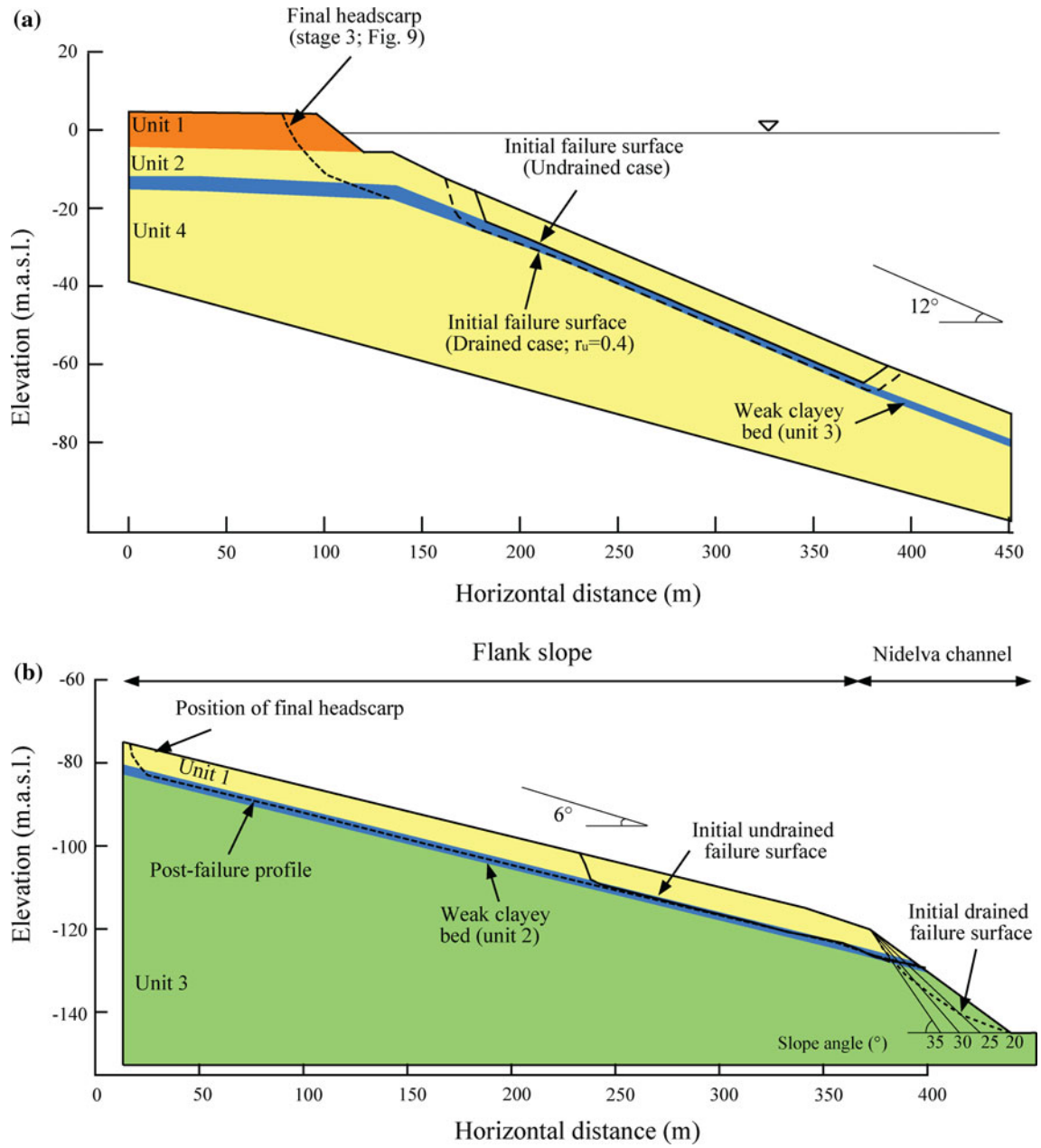

Fig. 7 Simplified model used for slope stability analysis with SLOPE/W for **a** the Brattøra landslide and **b** the W-landslide

potential failure surface) is calculated using the General Limit Equilibrium (GLE) method (Morgenstern and Price 1965; Fredlund and Krahn 1977).

The analysis of both landslides requires morpho-stratigraphic models (i.e. pre-landslide geometry) and estimates of geotechnical properties of the sediments. For the Brattøra site, a four-unit geological-geotechnical model is used to evaluate the stability of slopes prior to 1888 (Fig. 7a). A series of models with different slope angles (i.e. 7°, 10°, 12° and 15°) were created in order to evaluate the effect of slope geometry. These gradients are comparable to the present shoreline slopes and also similar to pre-landslide bathymetrical observations (Skaven-Haug 1955). The sediment is subjected to both drained and undrained loading conditions. This allows for the evaluation of different triggering mechanisms (e.g. placement of fill, rapid change in slope geometry, and/or tidal drawdown). In the undrained analysis, the weaker clayey bed (unit 3) is subjected to undrained loading with the s_u profile taken directly from CPTU-1 (Table 1). Long term strength reduction in the weak clayey bed (unit 3) is also considered as this layer has shown to be sensitive in core nearby (sensitivity ranging from 5 to 7). This was performed by dividing the undrained shear strength directly by the

Table 1 Physical and strength parameters used during the stability analyses at the W- and Brattøra sites

	Thickness (m)	γ (kN/m^3)	φ' (°)	c′ (kPa)	S_u at the top of layer (kPa)	ΔS_u (kPa/m)	Data from
Brattøra							
Unit 1: Coarse sand and gravel	10	22.0	37	–	–	–	CPTU-1 and CPTU-2
Unit 2: Loose silty sand	6–15	20	35	0	–	–	
Unit 3: Weak clayey bed	2	19	33[a]	6[a]	13,5	3	
Unit 4: Loose silty sand	>10	20	35	0	–	–	
W-landslide							
Unit 1: Silty sand	5	20	35	0	–	–	Core GS08
Unit 2: Weak clayey bed	2	19	33[a]	6[a]	8,0	2	
Unit 3: Clayey silt	>10	19	35	2	21,0	4	

[a] Mohr-Coulomb drained strength parameters obtained from triaxial tests on clayey samples from core GS08 (see Fig. 6c)

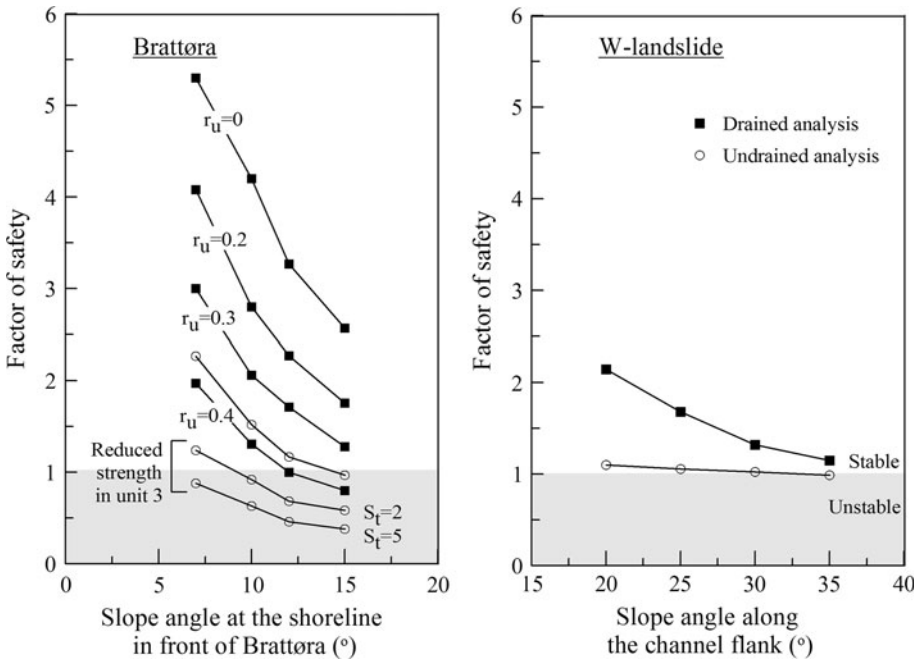

Fig. 8 Results from slope stability analysis for the Brattøra and W- slopes. Results from undrained analyses are presented with circles while the results from drained analyses are shown with squares. For the Brattøra site, the effect of changing the pore pressure ratio (r_u) on the factor of safety is shown. Similarly, the effect of long-term strength reduction (due to sensitivity; S_t) in the weak layer is shown. The location of slip surfaces for the Brattøra and W- slopes is shown in Fig. 7

sensitivity (S_t) of the clayey beds. In all analyses (i.e. drained and undrained analysis), the coarser and more permeable units 1, 2 and 4 are given drained strength parameters derived from CPTU-1 and CPTU-2 (Table 1). Moreover, data from groundwater monitoring on-shore near Brattøra shows that the excess pore pressure conditions may be significant within and immediately below the weaker clayey beds. This is considered in the drained stability analyses of the Brattøra slope. The role of pore pressure (u) is evaluated here using the pore pressure ratio (r_u) calculated using the unit weight of the sediments (γ):

$$r_u = u/\gamma h \tag{3}$$

where h is the thickness of the material above the potential failure plane.

For the back-analysis of the W-landslide, sedimentological and geotechnical data obtained from core GS08 are assumed to be representative of the mobilized sediments during the W-landslide (Table 1). The resulting geological-geotechnical model uses 3 units as shown in Fig. 7b. As seen from seafloor morphology (Fig. 4a), rapid erosion along the channel flank may have triggered the W-landslide. Therefore, the pre-failure geometry varies the lower slope section near the channel flank from 20° to 35°, in order to study the effect of toe erosion on the stability of the slope (Fig. 7b). In the landslide scar area, the slope gradient is assumed to be constant and parallel to layers in the stratigraphy, at an angle of 6° (Fig. 7b). This assumption is justified by seismic data that show nearly uniform sediment thicknesses in undisturbed sections draping the

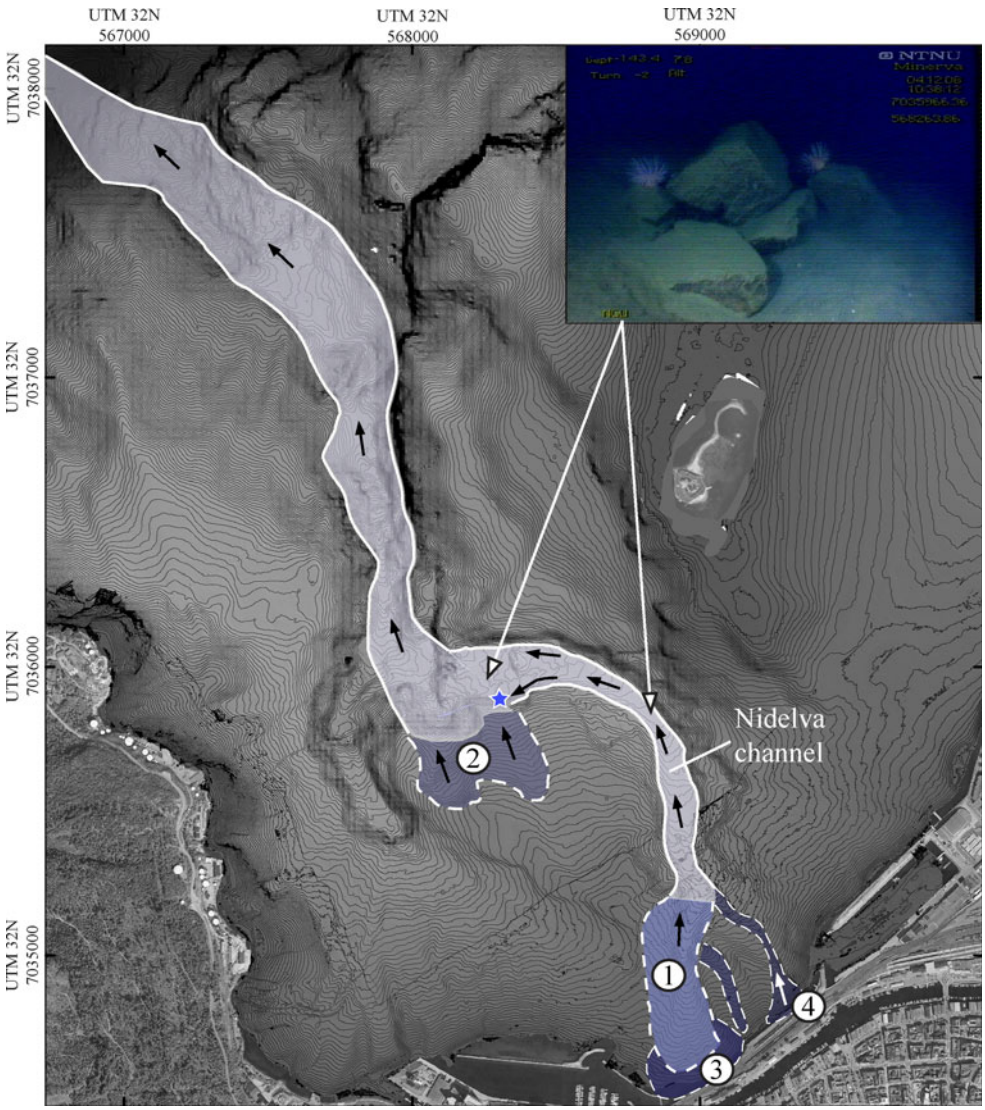

Fig. 9 Conceptual sequence of events in 4 stages. 1- Initial shoreline landslide outside Brattøra, 2- Undercutting of the channel flank (at the blue star) and triggering of the W-landslide also causing the tsunami wave, 3- Failure of the railway station and embankment fill along the shoreline of Brattøra as the flood wave receded from the shore, and 4- Slope failure to the east of the main landslide some hours following the event. Pictures from ROV observations show that during stages 3 and 4 large rock blocks from the breakwater structure located at Brattøra were transported at least 2 km offshore through the Nidelva channel

slope adjacent and upslope of the landslide (Fig. 6a). Hydrostatic groundwater conditions are assumed in the analysis of the W-landslide.

Results

For undrained loading conditions, the Brattøra slope is modelled to be stable until a gradient of 15° is reached (Fig. 8). For all undrained simulations the most critical failure surface passes through the top of the weak clayey bed (Fig. 7a). For the case where we consider a strength reduction of 2 (i.e. $S_t = 2$), the slope is modelled to be metastable (i.e. the factor of safety is below unity) if steeper than 9° (Fig. 8). In addition, when using a sensitivity of 5 (similar to that measured in cores nearby), all the modelled slopes present factor of safety below unity (Fig. 8). Alternatively, results from drained analysis show that the shoreline slope is unstable when using slope gradient greater than 12° and a pore pressure ratio similar to that measured onshore at Brattøra ($r_u = 0.4$) (Fig. 8). The most critical failure surface in the drained analyses is located at the interface between unit 3 and 4 (Fig. 7a), due to high pore pressure at this location.

The W-slope is modelled for both drained and undrained conditions. For the drained case (i.e. long-term situation along the Nidelva channel), results show that the W-slope is stable (FoS > 1.2) for the range of modelled slope geometries (Fig. 8). The most critical failure surface is shallow and situated along the channel flank (Fig. 7b). Such a failure mechanism does not agree with the observed morphology of the W-landslide scar and is therefore unlikely (Fig. 4a). On the other hand, the undrained slope stability analysis simulates the short-term situation of a slope. This may represent, for example, a sudden undercutting at the base of the slope along the submarine channel. Results from the undrained analysis show that

failure occurs for channel flank slopes steeper than 30° (Fig. 8). Initial failure develops at the top of the weak clay-rich bed where the undrained shear strength is lowest (Fig. 7b). The geometry of this undrained failure surface agrees well with the morphology of the W-landslide (Fig. 4).

Discussion: the 1888 sequence of events

The results and observations presented above, combined with witness testimonies, are used to decipher the causes and mechanisms which led to the 1888 landslide and tsunami. The sequence of events, as discussed below, is also illustrated through 4 stages in Fig. 9.

At first, stability analysis performed on the near-shore slopes seaward of Brattøra testify for metastable conditions prior to 1888. A combination of steep slope angle and unfavourable groundwater conditions, due to intense spring snow melting and large tidal drawdown, may have been sufficient to trigger an initial near-shore underwater landslide (Stage 1—Fig. 9). The failure-prone clayey beds play an important role in this mechanism as their great lateral extent, combined with their inherent low-permeability, allows for the formation of artesian groundwater pressure at different stratigraphic levels (due to the general land-fjord groundwater flow). This is supported by measurement of artesian pore pressure on-shore at Brattøra and further evidenced by the presence of pockmarks on the seafloor. Such pockmarks features are often associated to fluid seepage processes (Hovland et al. 2002). In addition to the groundwater forces, high deviatoric loads (from the harbor extension and railway station constructed in 1880) may have enhanced strain accumulation in the sensitive clayey layers over time. Such a mechanism may have gradually reduced the soil's strength and the stability of the near-shore slopes. As seen from the results of the stability back-analyses presented in Fig. 8, only a small decrease in s_u in the weaker clayey beds has a large effect on the stability of the slope off Brattøra. A similar strength reduction mechanism has also recently been proposed for the 1979 Nice airport slope failure (Dan et al. 2007).

As the underwater sediments started moving downslope, unloading of the headwall and sidewalls subsequently caused a retrogressive landslide mechanism seaward of Brattøra. Retrogression continued upslope as long as favourable soil conditions and layer orientation existed, and as long as the morphology of the landslide area allowed for the evacuation of debris. The retrogressive process may have gradually ceased along the shore due to higher undrained shear strength in the clayey beds (due to greater burial depth) and to the presence of coarse littoral deposits and man-fills (cf. Fig. 2). The mobility of these materials is low and will tend to support the sidewalls. As shown from the more recent Pir-landslide event, an initial near-shore underwater landslide may have occurred outside Brattøra in 1888 without being registered. This is also similar to the 1990 landslide event which took place in the western part of the bay (Fig. 1). In this event, an initial underwater landslide ruptured cables on the fjord bed and sections of the shoreline slumped into the fjord only several hours following the initial landslide (Emdal et al. 1996, L'Heureux et al. 2007). Contrary to Skaven-Haug (1955) and Bjerrum (1971), we thus suggest that the 1888 event sequence in Trondheim started underwater, near-shore, following a detachment in the vicinity of a weak clayey bed (Stage 1—Fig. 9).

The morphology of slide scars outside Brattøra indicates that parts of the foreslope disintegrated following the failure and that the sediments were funnelled into the submarine channel (Fig. 4). Given the sea bed morphology and position of bedrock exposures, the resulting mass flow diverted towards the flanks of the Nidelva channel. This produced enhanced erosion and undercutting, in particular at the base of the "W"-landslide (Fig. 4, see also blue star in Fig. 9). As the Nidelva channel has not been linked to a major fluvial source since 3000–2000 cal. years BP (L'Heureux et al. 2009a), the area may have stabilized as erosion ceased. An external event, such as mass flow from an initial landslide seaward of Brattøra, may have been necessary to ultimately trigger the "W"- landslide (Stage 2—Fig. 9). This is supported by results from slope stability analysis presented above.

Compared to the near-shore area, the succession above the weak layer in the vicinity of the "W"-landslide is finer grained due to its distal deltaic location. Therefore, the rapid unloading of the "W"-slope likely triggered a translational landslide evacuating into the Nidelva as a compact debris flow with visco-plastic properties (see e.g. Elverhøi et al. 2010). The clean surface exposed in the W-landslide suggests the failure developed rapidly, much like what has been modelled for the Storegga slide (Kvalstad et al. 2005) and the Currituck slide (Locat et al. 2009). A combination of large failed sediment volumes, relatively steep slopes, restricted evacuation path and acceleration potential may have caused a large water displacement and the tsunami wave.

Tsunami simulations

The interpretation of the W-landslide as the cause for the 1888 tsunami in the bay of Trondheim is here further tested by making use of tsunami simulations. First, the volume and the runout of the "W"-landslide are prescribed inputs

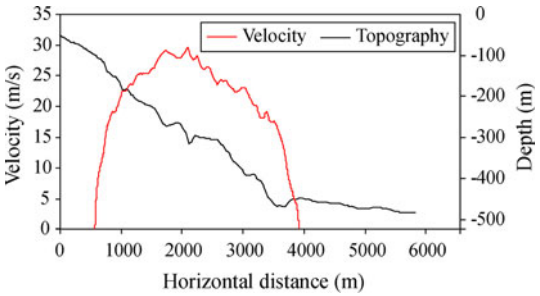

Fig. 10 2D bathymetric profile of the Nidelva Channel (from the location of the "W"-landslide to the deep fjord basin) and frontal flow velocity from the 2D-BING model (from L'Heureux et al. 2009b)

from the observations. There are of course no observations of the acceleration, the velocity, or the general landslide behaviour. Hence, the failed mass is modelled as a deformable visco-plastic Bingham fluid applying the two-dimensional BING model (Imran et al. 2001). In other words, the landslide moves as a plug flow riding on top of a shear layer with a thickness determined by flow height and yield stress of the material. The two-dimensional (2D) model assumes that the sediments disintegrated and liquefied instantly upon failure. The landslide is initially given a depth of 8 m and a length of 320 m based on the morphological data. The yield strength is set to 50 Pa (L'Heureux et al. 2009b). In Fig. 10 the frontal flow velocity of the landslide is shown. The applied rheological parameter (i.e. yield strength of 50 Pa) might be too low (the value is enforced to get the slide started in the BING model), and as a result the velocities might be too high. However, the volume and the initial acceleration are more important than the velocity for the resulting tsunami (Løvholt et al. 2005).

Most tsunami simulations are accomplished in two horizontal dimensions (2HD) for sea-surface elevation and depth-averaged horizontal wave current speed, by solving the linear and non-dispersive (hydrostatic) shallow-water (LSW) equations for conservation of mass and momentum (Mei 1989). In these equations, it is assumed that characteristic sea-surface elevation of the waves (i.e., deviation from equilibrium water level), is much less than typical water depth. In addition, it is assumed that the characteristic wavelength is much longer than typical water depth. However, for the cases where the waves are shorter (as in the present case) the pressure is no longer hydrostatic and the waves will be influenced by dispersive effects implying that the speed of wave propagation depends on the wave length; longer waves travel faster than shorter ones. Furthermore, if the characteristic amplitudes are higher than in the LSW regime above, the waves may be influenced by non-linearity. This effect can be seen, e.g., as steepening of waves propagating towards the shore, followed by possible wave breaking. To include these two higher order effects (dispersion and non-linearity) we apply so-called Boussinesq models (Mei 1989). In the present work, we applied the Boussinesq model called *GloBouss* (Pedersen and Løvholt 2008; Løvholt et al. 2008; 2010).

In the tsunami model, the landslide is simplified as a flexible box with a prescribed velocity progression deduced from the BING model landslide simulations (cf. Fig. 10). The maximum velocity (about 30 m/s) is reached after 1400 m, and the slide has come to rest after a distance of about 3200 m. The "box-slide" is rounded to avoid numerical noise caused by sharp edges, with physical dimensions of 1.32 × width (430 m) × height (8 m) × length (320 m) or approximately 1.45×10^6 m^3. A factor of 1.32 comes from the applied rounding of the landslide. In the tsunami model, landslide propagation follows a straight line (L'Heureux et al. 2009b) and the tide is not taken into account. In light of the overall uncertainty (landslide parameters, etc.), these models give reasonable results for tsunami propagation. For further details on landslide representation we refer to Harbitz (1992) and Løvholt et al. (2005).

In Fig. 11a, b, the surface elevation of the tsunami generated by the "W"-landslide is shown after 2 and 5 min, respectively. The maximum surface elevation during the simulation period is shown in Fig. 11c. Inside and close to the area of the sliding masses the surface elevations are more than 10 m, and attenuate down to below 1 m in the central part of Trondhjemsfjorden. Close to the shoreline on the northern side of the fjord, the waves amplify from less than 1 m up to about 2 m. The amplification here is due to shoaling.

To reveal the effects of dispersion and non-linearity, we compared time series of the surface elevation at synthetic gauges at different locations in the fjord (see Fig. 11 for the locations). Figure 12 reveals the results for gauges located outside Brattøra (gauge 1) and Rørvika (gauge 3). At Brattøra the first wave is a depression formed by the sediment removal (the tail of the landslide) prior to the arrival of the wave peak formed above the front of the landslide. However, outside Rørvika, the first wave is a positive peak created by the landslide front. The effect of dispersion is clearly seen when comparing the results of the different mathematical descriptions (see Fig. 12 where lower and smoother waves for the dispersive solutions are shown). For the leading waves we may conclude that the dispersive effect is more pronounced for waves propagating over longer distances, giving a slightly different (and smoother) solution and reduced surface elevations. At Brattøra close to the landslide area, the effect of dispersion is more or less absent for the leading waves due to short time of influence of dispersion (and shallower water). In addition, there is no significant effect of non-linearity. However, as we will see below, non-linear effects are important during inundation.

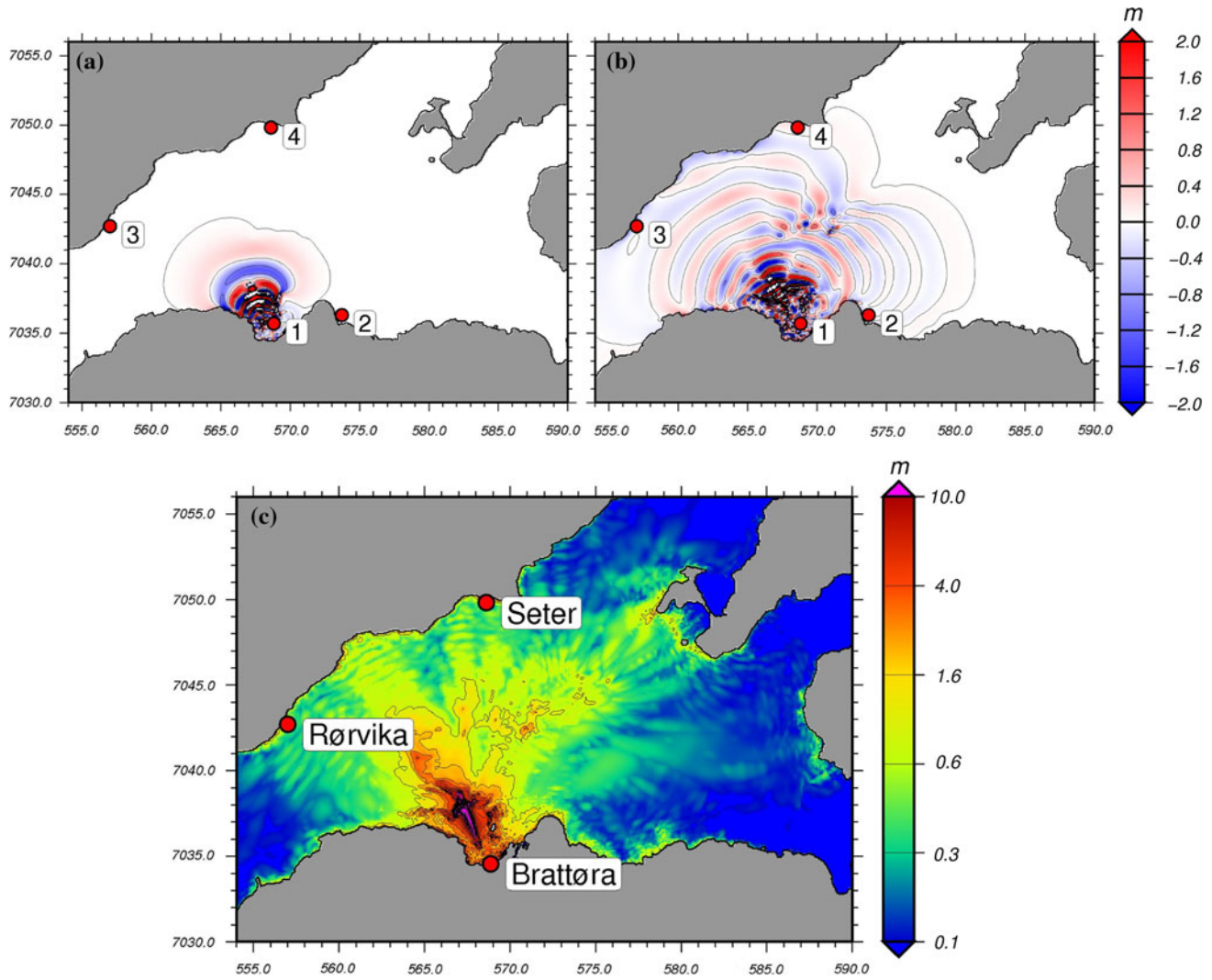

Fig. 11 Results from tsunami simulation showing **a** surface elevation after 2 min, **b** after 5 min and **c** maximum surface elevation during the total simulation time. The locations of the gauges 1–4 are shown

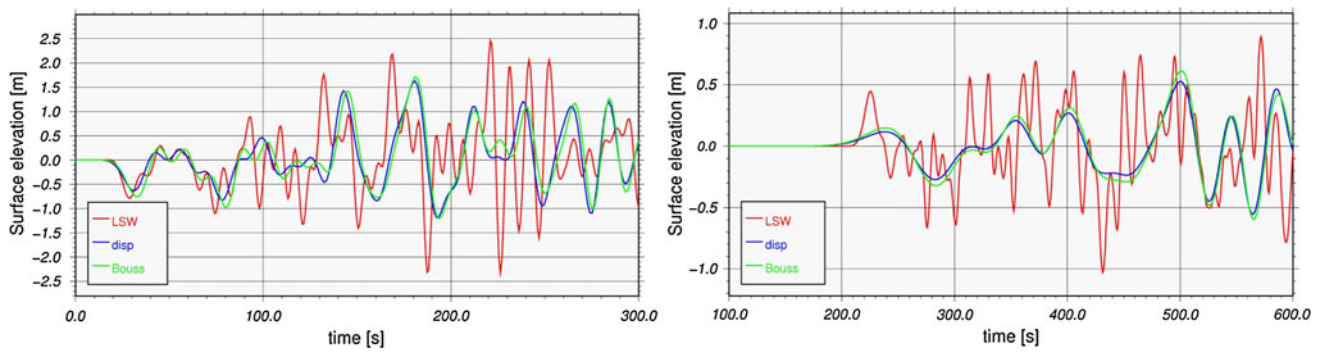

Fig. 12 Time history results of surface elevations outside Brattøra (gauge 1; Fig. 11) and Rørvika (gauge 3; Fig. 11) for different mathematical descriptions as explained in the text. The legends "LSW", "disp", and "Bouss" reflect the linear hydrostatic, the linear dispersive, and the full Boussinesq descriptions (including both dispersion and non-linearity), respectively

The tsunami inundation is calculated using the standard model ComMIT/MOST (ComMIT 2010; Løvholt et al. 2010). The surface elevation and velocity components from the tsunami propagation (linear dispersive description) above are given as input to the model. The maximum surface elevations (offshore) and inundation heights (on

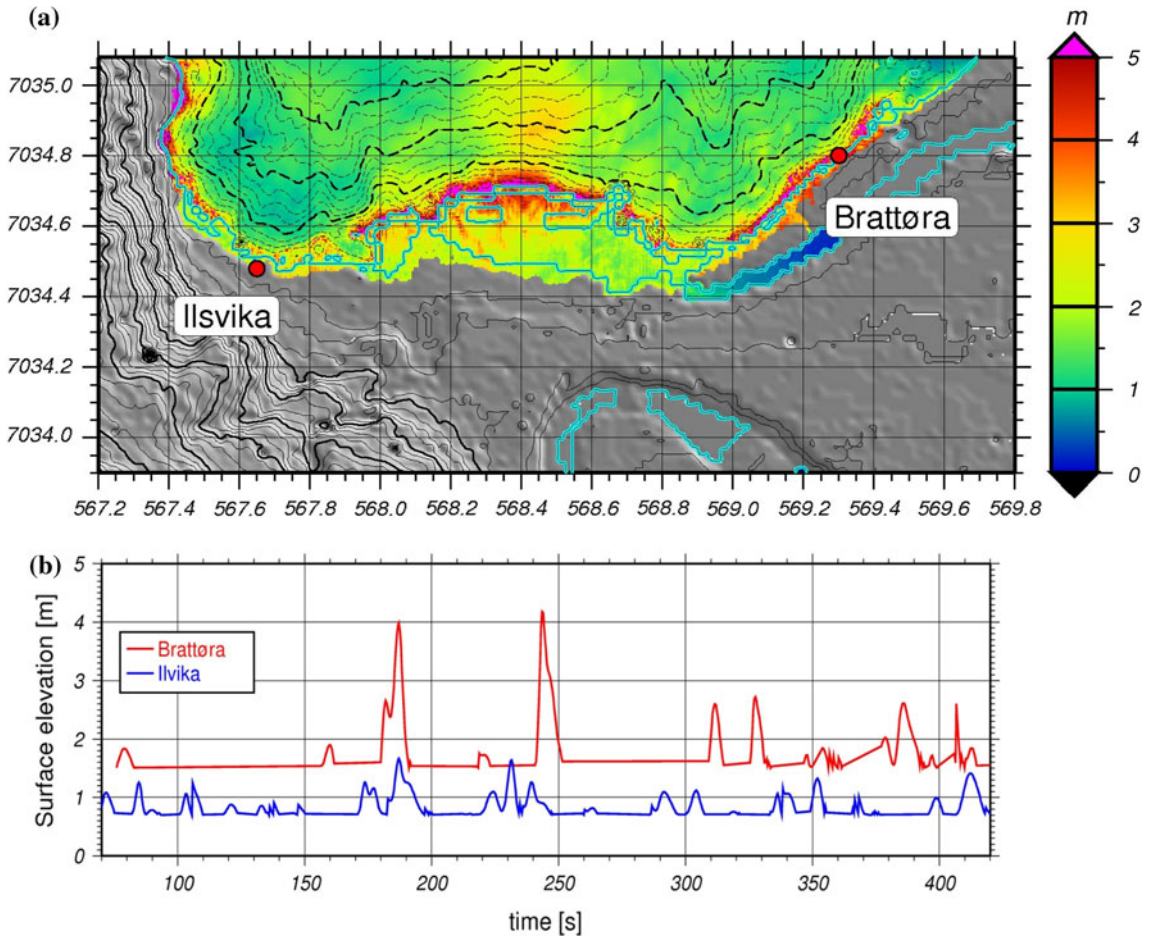

Fig. 13 **a** Maximum surface elevation and inundation height given in meters from tsunami simulations. The shoreline at equilibrium is coloured *cyan*. The contour lines for bathymetry and topography are drawn for every 5 m and 20 m using *thin* and thick lines, respectively (*dashed lines* are applied for the bathymetry). **b** Time history results of the surface elevation during run-up for the red bullets at Brattøra and Ilsvika

land) are shown in Fig. 13a. Outside the breakwater the waves are breaking due to non-linear effects, leading to a reduction of the surface elevation. On land the maximum inundation heights are up to 4–5 m.a.s.l. Time history of the surface elevations (on land and close to the shoreline, see the red bullet points in Fig. 13a for the locations) are presented in Fig. 13b. The numerical simulations show that the waves arrives Ilsvika slightly before reaching Brattøra. The highest simulated wave gave an inundation height of 4–5 m, which is in good agreement with the measured run-up height of 5–7 m from 1888 (Bjerrum 1971). Beyond the fact that the eyewitnesses described a wave approaching the shore from mid fjord, this confirms that the 1888 tsunami was generated by the "W"-landslide as the initial near-shore landslide/debris flow (i.e. stage 1) would most likely have too small volume to generate the observed 1888 tsunami.

The water exposure on land at Brattøra lasts up to 20 s for the impact of the two highest waves (Fig. 13b). In this area, the stability of the near-shore slopes and embankment fill was greatly reduced following the initial landslide (i.e. Stage 1—Fig. 9). Therefore, the tsunami wave caused important damages at Brattøra alone. As the wave receded, part of the railway station slumped into the fjord (Stages 3 and 4—Fig. 9). It remains to be shown whether the lowering of the water level associated with the tsunami (i.e. increase in deviatoric stresses) and duration of the inundation were sufficient to trigger the observed final near-shore landslides/debris flows from the upper part, or whether they possibly developed retrogressively from below the sea surface following Stage 1. There is also evidence of strong current velocities and potentially erosive sedimentary flows in the final stages of the event with the findings of sediment waves on the seafloor, a scour feature in the landslide scar at Brattøra, and large rock blocks transported more than 2 km on the floor of the Nidelva Channel (Fig. 9). These blocks most likely originated from the breakwater and embankment fill at Brattøra which failed in stages 3–4 in 1888.

Implications for hazard assessment in near-shore environments

When assessing the hazard potential from near-shore landslides, not only the process leading to failure of the soil mass is of concern, but also the post-failure behaviour of the displaced mass. As shown from the present study of the landslides in the bay of Trondheim, a single slope failure can develop into an erosive gravity flow and affect large areas of the seafloor downstream. However, out of three large historical slope failures in the Trondheim harbour, only the 1888 event caused a tsunami wave. The reason for this may be associated to the fact that the initial landslide was located immediately at the head of a large submarine channel. The initial sedimentary flow was directly funnelled into the channel and it had the opportunity to affect several slope sections downstream by axial incision. Slope failure along steep channel walls may furthermore have a larger tsunamigenic potential due to acceleration potential and the restricted evacuation path of the landslide masses. The potential hazard posed by mass movement processes must therefore be assessed regionally when planning construction activity in near-shore and coastal environments.

Conclusions

The 1888 shoreline landslide and tsunami in the bay of Trondheim is a good illustration of submarine, multiphase land-sliding in near-shore environments that can generate tsunamis. The integration of seafloor morphology with a dataset of cores, CPTU tests and slope stability analysis shows that the near-shore slopes had a relatively low stability prior to 1888 owing to the presence of a soft clayey layer in the steep delta foreslope. Initial land-sliding most likely occurred as a detachment along or close to a weak clayey bed due to unfavourable groundwater conditions (i.e. low tide, high groundwater seepage forces from intense snow melting) and possible strain accumulation in the sensitive clayey layers over time. The landslide rapidly transformed into a debris flow which facilitated additional slope failures, in particular the W-landslide on the flanks of the Nidelva submarine channel. Modelling of landslide dynamics and tsunami simulations indicate that the volume and acceleration of the "W"-landslide caused the 5–7 m high flood wave which struck the shores of Trondheim on April 23rd 1888.

Acknowledgments Svein Hove and the Norwegian road authorities are thanked for access to CPTU data. Oddbjørn Totland is thanked for acquisition and processing of the geophysical data. We are also thankful to the crews of R/V Seisma, R/V Gunnerus and R/V G.O. Sars for invaluable assistance during data acquisition. We acknowledge financial contributions to this project from the Trondheim Harbor, the Norwegian road authorities, the International Centre for Geohazards (ICG), the Norwegian Geotechnical Institute (NGI), the Geological Survey of Norway (NGU), the Norwegian University of Science and Technology, and the Research Council of Norway (NFR). The authors are grateful to R. Urgeles and two anonymous reviewers for their helpful suggestions and constructive comments. This is contribution no. 307 of the International Centre for Geohazards.

References

Bjerrum L (1971) Subaqueous slope failures in Norwegian fjords. Norwegian Geotechnical Institute, Publ. No. 88

Campanella RG, Robertson PK, Gillespie D (1983) Cone penetration testing in deltaic soils. Can Geotech J 20:23–35

ComMIT (2010) Software and documentation. URL: http://nctr.pmel.noaa.gov/ComMIT/index.html

Dan G, Sultan N, Savoye B (2007) The 1979 Nice harbour catastrophe revisited: trigger mechanism inferred from geotechnical measurements and numerical modeling. Mar Geol 245: 40–64

Elverhøi A, Breien H, De Blasio FV, Harbitz CB, Pagliardi M (2010) Submarine landslides and the importance of the initial sediment composition for run-out length and final deposit. In: 70th anniversary of Prof. B.N. Gjevik ocean dynamics special issue. doi:10.1007/s10236-010-0317-z

Emdal A, Janbu N, Sand K (1996) The shoreline slide at Lade. In: Senneset K (ed) Landslides. Proceedings of the 7th international symposium on landslides, Trondheim, Norway, vol 1, pp 533–538

Fredlund DG, Krahn J (1977) Comparison of slope stability methods of analysis. Can Geotech J 14:429–439

GEO-SLOPE (2008) Stability modeling with Slope/W 2007: an engineering methodology, 4th edn. GEOSLOPE International Ltd, Calgary, 355 pp

Gölke M, Cloetingh S, Coblentz D (1996) Finite-element modeling of stress patterns along the Mid-Norwegian continental margin, 628 to 688N. Tectonophysics 266:33–53

Hansen L, L'Heureux J-S, Longva O (2010) Turbiditic, clay-rich event beds in fjord-marine deposits caused by landslides in emerging clay deposits – palaeoenvironmental interpretation and role for submarine mass-wasting. Sedimentology. doi:10.1111/j.1365-3091.2010.01188.x

Harbitz CB (1992) Model simulations of tsunamis generated by the Storegga Slide. Mar Geol 105:1–21

Hovland M, Gardner JV, Judd AG (2002) The significance of pockmarks to understanding fluid flow processes and geohazards. Geofluids 2:127–136

Imran J, Harff P, Parker G (2001) A numerical model of submarine debris flow with graphical user interface. Comput Geosci 27:717–729

Kongsberg Defense & Aerospace (2004) TOPAS PS 40, System specifications, Parametric sub-bottom profiler. Brochure PS 40. www.kongsberg.com

Kvalstad TJ, Andresen L, Forsberg CF, Berg K, Bryn P, Wangen M (2005) The Storegga slide: evaluation of triggering sources and slide mechanics. Mar Petrol Geol 22:245–256

L'Heureux J-S, Longva O, Hansen L, Vingerhagen G (2007) The 1990 submarine slide outside the Nidelva River mouth, Trondheim, Norway. In: Lykousis V, Sakellariou D, Locat J (eds) Submarine mass movements and their consequences. Kluwer Series on Advances in Natural and Technological Hazards Research, vol 27, pp 259–267

L'Heureux J-S, Hansen L, Longva O (2009a) Development of the submarine channel at the mouth of the Nidelva River,

Trondheimsfjorden, Norway. Mar Geol 260:30–44. doi: 10.1016/j.margeo.2009.01.005

L'Heureux JS, Longva O, Sylfest G, Hansen L, Harbitz CB, Gauer P (2009b) Causes for the 1888 shoreline landslide and tsunami in Trondheimsfjorden, Mid-Norway. In: Proceedings of the 1st international conference on seafloor mapping for geohazard assessment, 11–13 May 2009, Ischia Island, Italy

L'Heureux J-S, Hansen L, Longva O, Emdal A, Grande L (2010) A multidisciplinary study of submarine landslides at the Nidelva fjord delta, Central Norway–Implications for geohazards assessments. Norw J Geol 90:1–20

Dehls JF, Olesen O, Bungum H, Hicks E, Lindholm, CD, Riis F (2000) Neotectonic map, Norway and adjacent areas, 1:3 million. Geological Survey of Norway, Trondheim. URL: http://www.ngu.no/sokkelkart/Neotectonic_map.pdf

Locat J, Lee HJ (2002) Submarine landslides: advances and challenges. Can Geotech J 39:193–212

Locat J, Lee HJ, ten Brink US, Twichell D, Geist E, Sansoucy M (2009) Geomorphology, stability, and mobility of the Currituck slide. Mar Geol 264:28–40

Løvholt F, Harbitz CB, Haugen KB (2005) A parametric study of tsunamis generated by submarine slides in the Ormen Lange/Storegga area off western Norway. Mar Petrol Geol 22:219–231

Løvholt F, Pedersen G, Gisler G (2008) Oceanic propagation of a potential tsunami from the La Palma Island. J Geophys Res 113:C09026, doi:10.1029/2007JC004603

Løvholt F, Pedersen G, Glimsdal S (2010) Coupling of dispersive tsunami propagation and shallow water coastal response. Accepted for publication in Zahibo N, Pelinovsky E, Yalciner A, Titov V (eds) Proceedings of the "Caribbean Waves 2008" workshop in Guadeloupe, Dec. 2008. Open Oceanogr J 4:71–82

Lunne T, Robertson PK, Powell JJM (1997) Cone penetration testing in geotechnical practice. Spon Press (Taylor and Francis Group), 312 pp

Lysså A, Hansen L, Christensen O, L'Heureux J-S, Longva O, Olsen H, Sveian H (2007) Landscape evolution and slide processes in a glacioisotatic rebound area: a combined marine and terrestrial approach. Mar Geol 248:53–73

Mei CC (1989) The applied dynamics of ocean surface waves: advanced series on ocean engineering. World Scientific Publications, Singapore 760 p

Morgenstern NR, Price VE (1965) Analysis of stability of general slip surfaces. Geotechnique 15:79–93

Pascal C, Gabrielsen RH (2001) Numerical modelling of cenozoic stress patterns in the Mid Norwegian Margin and the northern North Sea. Tectonics 20:585–599

Pedersen G, Løvholt F (2008) Documentation of a global Boussinesq solver. Department of Mathematics, University of Oslo, Norway. URL: http://www.math.uio.no/eprint/appl_math/2008/01-08.html

Piper DJW, Asku AE (1987) The source and origin of the 1929 Grand Banks turbidity current inferred from sediment budgets. Geo Mar Lett 7:177–182

Prior DB, JM Coleman, Bornhold BD (1982) Results of a known instability event. Geo Mar Lett 2:117–122

Reite A (1995) Deglaciation of the Trondheimsfjord area, Central Norway. Geol Surv Norway Bull 427:19–21

Reite AJ, Sveian H, Erichsen E (1999) Trondheim fra istid til nåtid—landskapshistorie og løsmasser, Geological Survey of Norway. Gråsteinen 5, 40 pp

Robertson PK (1990) Soil classification using the cone penetration test. Can Geotech J 27:151–158

Senneset K, Sandven R, Lunne T, By T, Amundsen T (1988) Piezocone tests in silty soils. In: Proceedings of the international symposium on penetration testing, ISOPT-1, Orlando, vol 2. Balkema, Rotterdam, pp 955–966

Skaven-Haug S (1955) Undervannsskred i Trondheim havneomraade. Teknisk Ukeblad 102(7):(also in publ. 7, Norwegian Geotechnical Institute, Oslo, Norway, pp 133–144)

Statens Vegvesen (2004a) Ground investigations and revised data report: Ud-359B – E6 Nordre Avlastningsveg over Brattøra (in Norwegian)

Statens Vegvesen (2004b) Ground investigation and data report: Ud-359C - E6 Nordre Avlastningsveg Kulvert Under Skansenløpet (in Norwegian)

Statens Vegvesen (2008) Evaluation of groundwater and uplift pressure in Pit 5 – Skansenløpet tunnel. Unpublished internal report, 11 pp

Tappin DR (2009) Mass transport events and their tsunami hazard. In: Mosher DC, Shipp RC, Moscardelli L, Chaytor JD, Baxter CDP, Lee HL, Urgeles R (eds) Submarine mass movements and their consequences, advances in natural and technological hazards research, vol 28. Springer, Dordrecht, pp 667–684

Wolff CF (1976) Geologisk kart over Norge, berggrunnskart Trondheim 1:250.000. Geological Survey of Norway